Geomechanics and Engineering, *Vol. 40, No. 2 (2025) 111-122*
https://doi.org/10.12989/gae.2025.40.2.111

A test model and its application for studying the characteristics of subgrade mud pumping under cyclic loading of railways

Yu Jia[1], Yu Ding*[2,3], Xuan Wang[1,4], Jiasheng Zhang[1,4] and Xiaobin Chen[1,4]

[1]*School of Civil Engineering, Central South University, Changsha, Hunan 410083, China*
[2]*School of Civil and Ocean Engineering, Jiangsu Ocean University, Lianyungang, Jiangsu 222005, China*
[3]*Jiangsu Ocean Engineering Research Center for Intelligent Infrastructure Construction, Jiangsu Ocean University, Lianyungang, Jiangsu 222005, China*
[4]*National Engineering Laboratory for High-speed Railway Construction, Central South University, Changsha, Hunan 410083, China*

(*Received April 25, 2024, Revised December 24, 2024, Accepted January 18, 2025*)

Abstract. The problem of mud pumping in saturated subgrade seriously affects the safe operation of trains on railways. There are relatively few research results on the characteristics of subgrade mud pumping, and those that do exist dispute the precise mechanism of the mud pumping. In this paper, a new test model is designed to study the important characteristics of subgrade mud pumping. The model can monitor not only the evolution of subgrade mud pumping but excess pore water pressure and dynamic stress in soil as well. In particular, we study the mud pumping of Lean Clay. Our results show that with the increase in the number of cycles, the axial strain of samples increases rapidly and then slowly. The axial strain increases with the increase in cyclic loading amplitude and decreases with the increase in loading frequency and initial dry density of Lean Clay. We also find that the excess pore water pressure first increases rapidly and then decreases slowly with the increase in the number of cycles. Furthermore, with the increase in cyclic loading amplitude, excess pore water pressure increases, and with the increase in the initial dry density, the excess pore water pressure decreases. We find that the loading frequency has little effect on excess pore water pressure. After the test procedure, we find that an increase in cyclic loading amplitude aggravates the degree of Lean Clay subgrade mud pumping and that an increase in loading frequency and increase in initial dry density of subgrade soil reduces the degree of mud pumping. We further find that the upward migration of fine particles driven by excess pore water pressure gradient is the main mechanism of subgrade mud pumping. However, the generation of an interlayer can also promote the occurrence of subgrade mud pumping.

Keywords: axial strain; cyclic loading; excess pore water pressure; fine particle migration; mud pumping

1. Introduction

The rapid development of China's economy has brought with it increased demand for resource transportation, and heavy-haul railway freight in particular. The heavier axle loads of these trains increases the dynamic stress on the subgrade and frequently results in numerous disasters such as mud pumping, which is becoming a more and more serious problem. In 2002, an investigation into subgrade problems in the Xizhai-Shimen section of the Jiaozuo-Liuzhou Line showed that the length of the line where subgrade mud pumping occurred reached 16,144 m (Hu 2003). According to the statistical data from Shuozhou-Huanghua Railway in 2008, there were as many as 882 mud pumping sites (Miao *et al.* 2014). This rising trend underscores the urgent need to incorporate geological insights and dynamic stress analysis (Zhou *et al.* 2023, He *et al.* 2024).

The problem of mud pumping not only fouls the overlying ballast layer and damages the strength and drainage performance of the ballast layer (Nguyen and Indraratna 2021, Nguyen *et al.* 2019, Indraratna *et al.* 2013, Tennakoon *et al.* 2014, Hussaini *et al.* 2016, Indraratna *et al.* 2011). But also forms a weak interlayer between the subgrade and the trackbed, causing excessive plastic deformation, uneven settlement and misalignment of the trackbed, which seriously affects the capacity expansion and operation safety of heavy-haul railway (Trinh *et al.* 2012, Wheeler *et al.* 2017, Liu and Xiao 2010, Yang *et al.* 2021, Touqan *et al.* 2020, Cao *et al.* 2023).

The problem of mud pumping is widespread, and some researchers have thus already conducted studies on its characteristics. Duong *et al.* (2014a, b) developed a physical model to study mud pumping and the migration of fine particles in railway subgrade and concluded that saturated subgrade generates large excess pore water pressure under cyclic loading and that the dissipation of excess pore water pressure can drive the migration of fine particles, causing mud pumping. Here, the increase in excess pore water pressure led to the decrease in effective stress. The ballast is easy to penetrate into the subgrade layer and squeeze the particles of the subgrade soil into the pores of the ballast layer. The study of Abeywickrama *et al.* (2019) showed that under the action of a train load, subgrade with poor drainage can generate and accumulate

*Corresponding author, Ph.D.
E-mail: dingyu@jou.edu.cn

ISSN: 2005-307X (Print), 2092-6219 (Online)

Table 1 Physical and mechanical parameters of Lean Clay

Materials	G_s	ω_L / %	ω_p / %	ρ_{dmax} / (g/cm^3)	ω_{opt} / %
Lean Clay	2.64	33.42	16.64	1.81	14.7

excess pore water pressure, which causes upward migration of slurry as well as mud pumping. Cai *et al.* (2021) conducted an experimental study on the mechanism of silty clay subgrade mud pumping under traffic loads. These results show that the excess pore water pressure gradually accumulates under a cyclic load, and when the effective stress is zero, the phenomenon of transient liquefaction and mud pumping occurs. However, Takatoshi (1997) believes that suction is generated between the sleepers and the ballast when a train is unloaded. This suction draws fine particles into the ballast and thereby causes mud pumping.

At present, there are relatively few research results about the characteristics of mud pumping specifically, and there is also no consensus about the mechanism by which it occurs. Therefore, we develop a test model for study the characteristics and mechanism of subgrade mud pumping under cyclic loading. This model can monitor the characteristics of subgrade mud pumping as well as the evolution of axial displacement and excess pore water pressure under cyclic loading. We present a novel explanation of the mechanism of subgrade mud pumping, which has important value for ensuring the safety of train operation.

2. Materials and testing methods

2.1 Materials

2.1.1 Lean clay

From our literature investigation, briefly described above (Kamruzzaman *et al.* 2008, Alobaidi and Hoare 1999, Trani and Indraratna 2010a, Trani and Indraratna, 2010b; Boomintahan and Srinivasan 1988, Koohmishi and Azarhoosh 2020, Hasnayn *et al.* 2020, Chawla and Shahu 2016, Indraratna *et al.* 2009, Indraratna *et al.* 2010), the soil most prone to mud pumping usually has the following characteristics. First, the content of clayey particles in the mud pumping soil is usually greater than 10%, and the content of powder particles is usually greater than 20%. Second, the moisture content is in the range of 23% to 75%, and the plasticity index is in the range of 5 to 42.5, including low-liquid limit silt, low-liquid limit clay, and low-liquid limit and high-liquid limit clay. Third, the permeability coefficient of the mud pumping soil is in the range of 3.28×10^{-8} cm/s to 1.39×10^{-4} cm/s, which indicates mostly weakly permeable soil and impermeable soil. However, some soils with good permeability (greater than 1.0×10^{-4} cm/s) still have some mud pumping. Finally, the main mineral components of the mud pumping soil are illite, montmorillonite, and kaolinite.

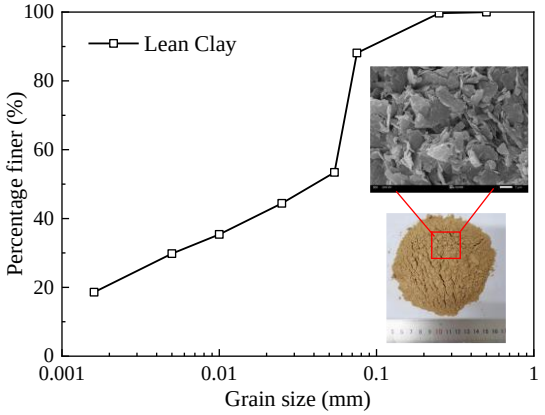

Fig. 1 Gradation curve of Lean Clay

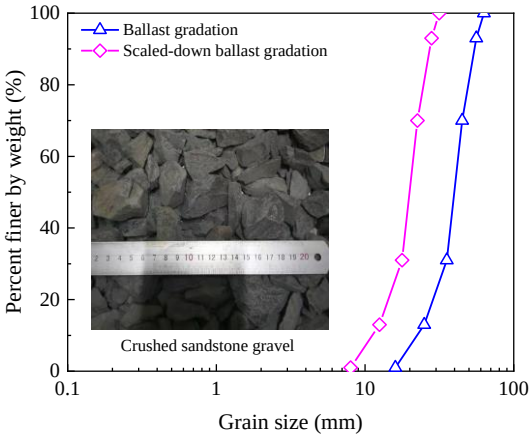

Fig. 2 Gradation curves of ballast

In this paper, clay was selected as the subgrade soil. The physical and mechanical parameters of clay were tested as shown in Table 1. Here we see that this clay can be classified as Lean Clay (CL) according to ASTM/USCS guidelines. The gradation curve of this Lean Clay and its Scanning Electron Microscope (SEM) images are shown in Fig. 1.

2.1.2 Gravel

Crushed sandstone gravel as shown in Fig. 2 was selected as the ballast. The specific gravity of the crushed gravel was 2.69 and the maximum dry density was 2.08 g/cm^3.

Limited by the size of our test instrument, the ballast gradation was scaled down 1/2 of full-scale ballast using the parallel gradation method (Indraratna *et al.* 1993, Wang 2017). Studies (Indraratna *et al.* 1993, Wang 2017) have shown that materials downscaled using this parallel gradation method can well represent the original materials in terms of mechanical properties. The gradation curves of the ballast and the scaled-down ballast are shown in Fig. 2. We can see that the non-uniformity coefficient and curvature coefficient of original ballast are 1.89 and 1.28, respectively. And the non-uniformity

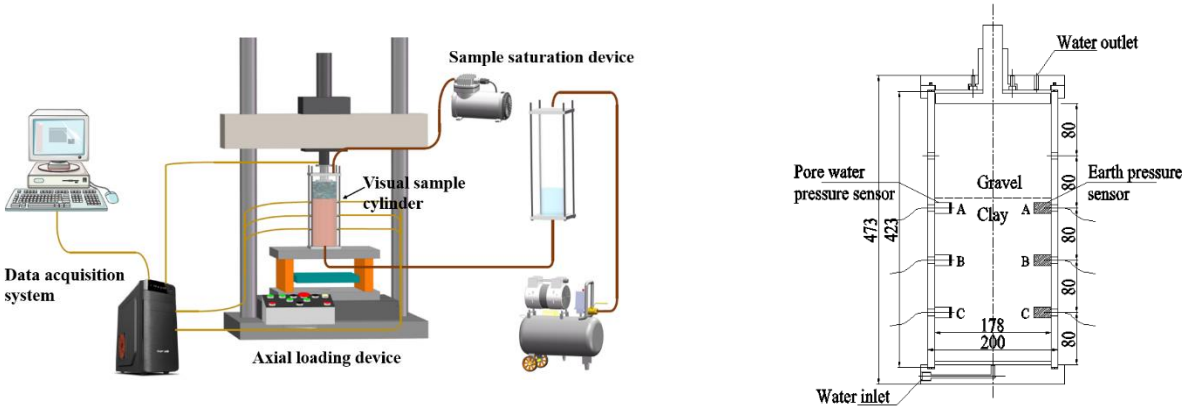

(a) Diagram of the test model (b) Diagram of sensor installation points

Fig. 3 The test model

coefficient and curvature coefficient of scaled-down ballast are 1.90 and 1.28, respectively. Therefore, the scaled-down ballast can well represent the original ballast. The scaled-down ballast is classified as poorly graded gravel.

The practice of designing many of existing heavy-haul railway lines in China is typically guided by the standards applicable to ordinary railways. Consequently, numerous railway track beds have been constructed directly atop suboptimal foundation conditions (Wang 2006, Yin 2012, Han 2018, Chen 2016). In this paper, the ballast is directly laid on the saturated subgrade soil during the test, in order to obtain obvious test results in a short time.

2.2 Test model and methods

2.2.1 Test model

The test model is composed of four parts (as shown in Fig. 3(a)): the axial loading device, the visual sample cylinder, the sample saturation device, and the data acquisition system. The axial loading device includes the reaction frame, the actuator, the servo valve, the hydraulic oil source and the digital controller. The static load and the dynamic load waveform that can be applied are 0-50 kN, and the accuracy is 0.1% of the maximum range. Additionally, the dynamic load that can take the form of a triangle wave, sinusoidal wave, square wave, random wave and other waveforms, and the dynamic load frequency range is 0-20 Hz.

The visual sample cylinder is made of high-strength Plexiglass, and the size of the sample cylinder is 178 mm (diameter) × 423 mm (height). The lower part of the sample cylinder has with an aluminum alloy bottom plate and a water inlet, and the upper part has with a loading plate, transmission column, sample cap, and upper water outlet. Importantly, the side wall of the sample cylinder has holes to install sensors (pore water pressure sensors and earth pressure sensors, installation points shown in Fig. 3(b)). Rubber sealing rings were installed at each connection part of the sample cylinder to ensure a good seal. The pore water pressure sensor with a range of 0-100 kPa, and the earth pressure sensor with a range of 0-200 kPa.

The sample saturation device is composed of a water tank, an air compressor, a vacuum pump, and other parts, which can vacuum and saturate the sample.

Finally, the data acquisition system can record the axial displacement, axial force, pore water pressure, earth pressure, and other data of the sample during the test in real time.

2.2.2 Test programs

A train load is usually simulated by a sinusoidal wave or a semi-sinusoidal wave (Bian *et al.* 2016, Tennakoon and Indraratna 2014). In this paper, a sinusoidal wave as shown in Fig. 4 was used. Before the cyclic load, an axial stress of 40 kPa was applied to simulate the influence of track structure's gravity. The reasons for choosing 40 kPa are as follows: firstly, we synthesized many research results on loading waveform of heavy-haul railway trains and ordinary railway trains, and concluded that the range of axial stress is about 20~50 kPa (Bian *et al*. 2016, Duong *et al.* 2014a, b, Gao *et al.* 2021, Cai *et al.* 2021, Han 2018). Secondly, it was found in the preliminary test that when the axial stress applied to the sample was too small, the sample was prone to penetration failure during the saturation process.

The amplitude and frequency of cyclic load are mainly affected by the axle load of the train, the running speed of the train, the length of the train, and the fixed distance of the train. The maximum dynamic stress on the ballast layer can be calculated with Eq. (1) proposed by Bian *et al.* (2016).

$$\sigma_{\mathrm{d}\max}=\frac{0.4P_{\mathrm{s}}(1+\alpha v)}{l\times b} \tag{1}$$

where $\sigma_{\mathrm{d}\max}$ is the maximum dynamic stress of the ballast layer, P_{s} is the axle load of the train, α is the dynamic impact coefficient, which is generally taken as 0.005, v is the running speed of the train, l and b are the length and width of the sleepers, respectively. For heavy-haul railways, the length and width of sleepers are generally 2.5 m and 0.25 m, respectively. According to Eq. (1), the maximum dynamic stress on the ballast layer exerted by a train with an axle load of 25 tonnes and a running speed of 80 km/h is about 224 kPa. The field dynamic test results of Datong-Qinhuangdao Line indicate that although dynamic stress on the foundation bed surface increases with both the axle load and the velocity of the train, the maximum dynamic stress amplitude recorded does not surpass 180 kPa (Yang 2015). The cyclic loading amplitudes used in this paper are 50 kPa, 100 kPa, and 200

Table 2 Testing programs

No.	Materials	Initial dry density ρ_d / (g/cm^3)	Cyclic loading amplitude σ_d / kPa	Frequency f/ Hz
CL-1.40-50-5	Lean Clay	1.40	50	5
CL-1.40-100-1		1.40	100	1
CL-1.40-100-5		1.40	100	5
CL-1.40-100-10		1.40	100	10
CL-1.40-200-5		1.40	200	5
CL-1.50-100-5		1.50	100	5
CL-1.59-100-5		1.59	100	5

Note: The method of test numbering is as follows: soil type-initial dry density-cyclic loading amplitude-frequency, for example: CL-1.40-100-5, represents a soil type of S (Lean Clay), an initial dry density of 1.40 g/cm^3, a cyclic loading amplitude of 100 kPa, and a frequency of 5 Hz

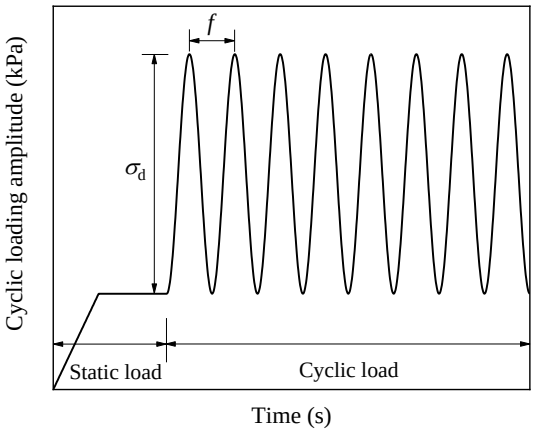

Fig. 4 Load oscillogram

Fig. 5 The sample after preparation

kPa. The frequency of cyclic load is calculated according to Eq. (2) (Sun *et al.* 2016)

$$f = \frac{v}{L} \tag{2}$$

where L is the wheelbase of the train. From Eq. (2), the frequency that corresponds to a train running speed of 0-100 km/h is 0-14 Hz, and the cyclic load frequencies used in this paper are 1 Hz, 5 Hz, and 10 Hz, respectively.

During the test the subgrade soil was in a saturated state, and the upper gravel layer was in an unsaturated state. All drainage valves were closed, and water was only allowed to seep upward along the gravel layer during the application of cyclic loading. The object of our test was subgrade soil, the depth of which is generally within the range of 0-2.5 m, and the confining pressure is relatively small. Therefore, the influence of confining pressure was not considered in this study.

The criterion for the end of the test was that the number of cycles reached 50,000 or the total axial strain of the sample reached 5%.

The testing program is shown in Table 2. After the test, the ballast layer was divided into three parts and then the particles sieving test was carried out. The gradation curves for each part were recorded and then compared with the gradation curve of gravel before the test (as shown in Fig. 2) to analyze the characteristics of subgrade mud pumping.

2.2.3 Test methods

The process of Lean Clay subgrade mud pumping test under cyclic loading could be divided into three stages: sample preparation, sample saturation, and loading.

The size of the sample was 178 mm (diameter) × 380 mm (height). The lower layer of the sample was filled with Lean Clay (subgrade) with a height of 250 mm, and the upper part was filled with gravel (ballast) with a height of 130 mm. Before filling the Lean Clay, it was necessary to lay two layers of filter paper on the lower part of the sample cylinder and open the water inlet valve to allow water flow over the surface of the filter paper to remove air. Then the water inlet valve was closed and evenly smeared Vaseline on the side wall of the sample cylinder. Vaseline can not only reduce the friction between the soil and the side wall but also prevent concentrated seepage along the side wall in the process of saturation. The Lean Clay was divided into five layers using the moist compaction method with manual hammering. Each layer had a thickness of 50 mm. The mass of each layer of soil was calculated according to the preset initial dry density and the optimal moisture content. During the process of compaction, the height of the falling hammer for each layer was controlled the same as far as possible. Before filling the next layer of soil, the surface of the compressed soil was scraped to ensure good contact between the layers. The upper

gravel was divided into three layers for filling. The thickness of the first two layers was 50 mm, and the thickness of the last layer was 30 mm. The compactness of ballast is about 1.75 g/cm^3. In the process of ballast compaction, only shallow indentation is formed on the surface of subgrade soil, which can be ignored compared with the thickness of interlayer generated during the application of cyclic load as shown in Fig. 7.

After the sample preparation was completed, we installed the loading plate, the pillar, and the upper sample cap and tightened the bolts to ensure a good seal, before starting the saturation process using a vacuum pump to pump air out of the sample for about 30 minutes at first. Next, the water inlet valve of the base was opened to make the water inside the water tank flow into the sample slowly. When the water surface was higher than the interface between the subgrade soil and gravel, the water inlet valve was closed. The test was carried out after letting the sample stand for 24 h. During the saturation process, a static load was applied to the upper part of the sample to prevent the soil from infiltration damage. Our previous test process found that the saturation of the Lean Clay can be greater than 0.90 after 24 hours of saturation. Finally, the cyclic loading pre-set was applied to the sample. The sample after preparation was shown in Fig. 5.

3. Test results

3.1 Analysis of typical test curves

Fig. 6 shows the curves of axial strain (ε), excess pore water pressure (u_d), and dynamic stress in soil (σ) during the mud pumping test of CL-1.40-200-5. Fig. 6(a) shows that the axial strain of the sample increases nonlinearly with the increase in the number of cycles. At the initial stage of cyclic loading (number of cycles less than 1000), the axial strain of the samples increases linearly with the increase in the number of cycles, and as the cyclic loading continues to be applied (number of cycles more than 1000), the axial strain of the sample continues to increase. However, this rate of increase gradually decreases until the end of the test, but the axial strain of the sample still does not reach a stable value. At the initial stage of cyclic loading, the gravel layer is pressed into saturated subgrade that forms an interlayer (see Fig. 7 for details. After the cyclic loading is applied, the gravel particle ① shows significant downward displacement, and the gravel layer sinks down to form an interlayer with a thickness of 14 mm) that results in a large axial displacement. As the cyclic loading continues to be applied, with the dissipation of excess pore water pressure (as shown in Fig. 6(b)) and the migration of fine particles (as shown in Fig. 7 with the application of cyclic loading, the liquid level and the mud rises), the axial deformation of the sample continues to increase.

As presented in Fig. 6(b), the excess pore water pressure increases rapidly to its maximum value and then decreases slowly with the increase in the number of cycles. Additionally, for the same number of cycles, the excess pore water pressure increases with the increase in soil depth. According to Fig. 7, due to the compressive deformation of saturated subgrade soil at the initial stage of cyclic loading, the excess pore water

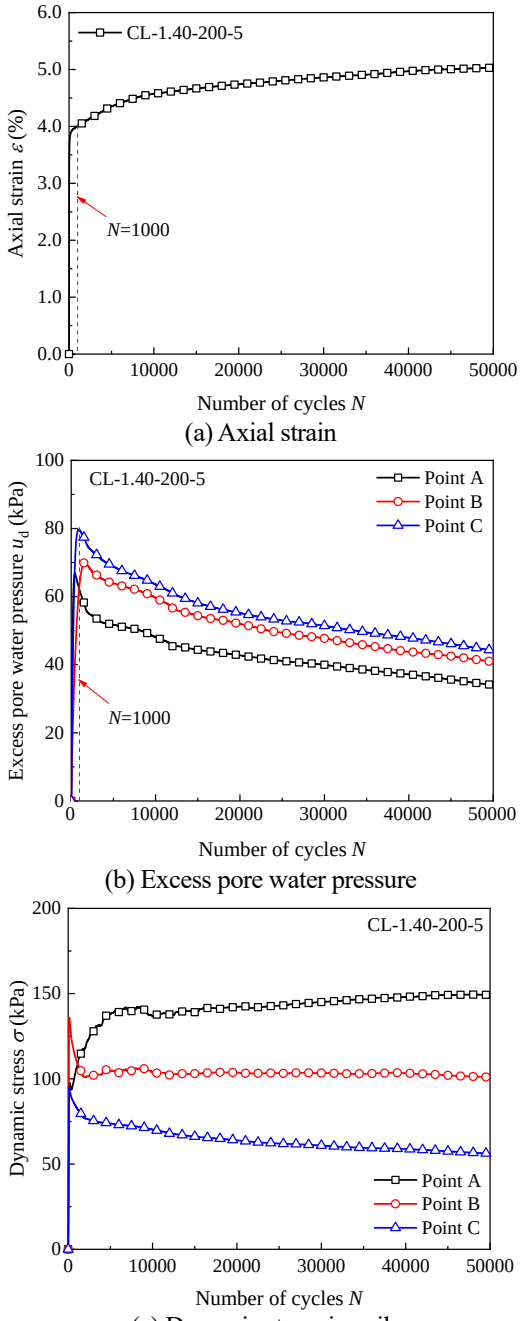

Fig. 6 Curves of axial strain, excess pore water pressure, and dynamic stress in soil

pressure inside the sample accumulates and gradually rises. Subsequently, the excess pore water pressure dissipates upwards along the gravel layer.

As shown in Fig. 6 (c), with the increase in the number of cycles, the dynamic stress in soil at points B and C decreases rapidly at first and then slowly. The variation of the dynamic stress at point A is inconsistent with that at points B and C, showing first a rapid increase and then only a slow increase. There are has some irregular data pattern for early loading cycles for Point A and Point B, and similar phenomena also exist in other experiments, especially at point A. This is attributed to the location of the earth pressure sensor at Point A, which is located below the interface between the gravel layer

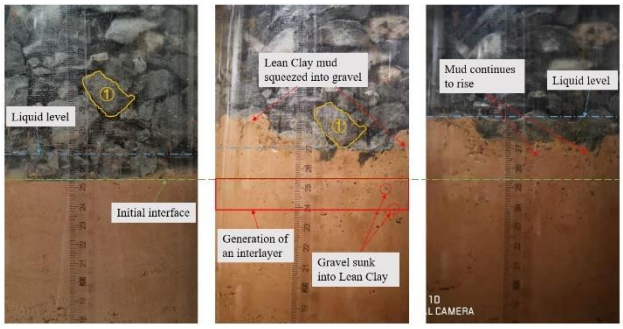

After saturation→After loading→At the end of test

Fig. 7 Change of soil-gravel boundary in CL-1.40-200-5 test

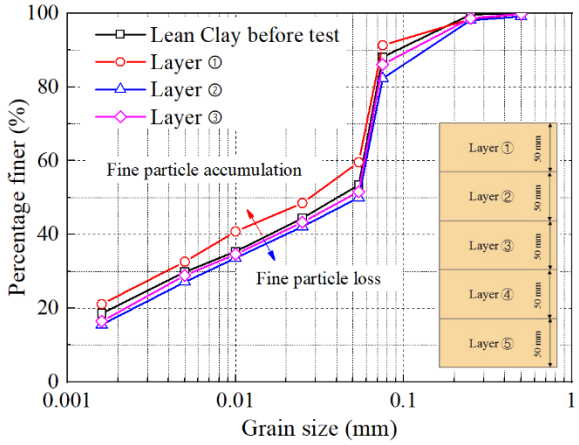

Fig. 8 Gradation curves of subgrade soil after testing

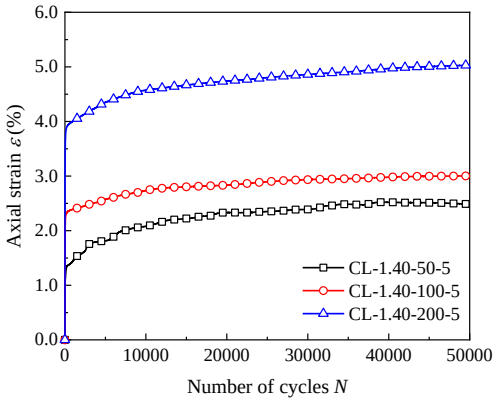

(a) Axial strain

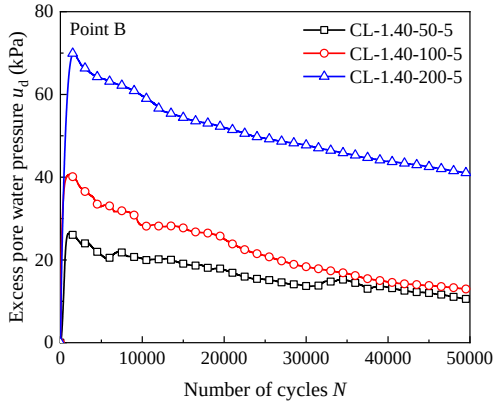

(b) Excess pore water pressure (point B)

Fig. 9 The influence of cyclic loading amplitude

and the subgrade. During cyclic loading, an interlayer can easily form at this location. Consequently, gravel particles that penetrate into the subgrade can impact the precision of the earth pressure sensor's readings. In addition, the dynamic stress in soil decreases with the increase in soil depth. The test data were cleared before the loading was applied, and the stress in Fig. 6(c) does not include the gravity stress of subgrade soil. In addition, the influence of dynamic loading on shallow subgrade soil is greater, and with the increase of subgrade soil depth, the influence of dynamic loading decreases (Zhang *et al.* 2020, Phong 2015, Liu, 2021).

Fig. 7 shows the change of soil-gravel boundary in CL-1.40-200-5 test. We can see that there is a clear initial interface between the subgrade soil and the ballast after the sample was saturated. When cyclic loading is applied to the sample, the gravel sunk into the weak subgrade soil and squeezed part of the mud into the gravel pores, and formed an interlayer. With the continuous application of cyclic loading, the mud continues to migrated upward, and the height of the liquid surface in the sample continues to rose. However, there were no mud overflowed to the surface of the ballast layer after the test. The main reasons are: (1) the number of cycles applied to the sample is only 50,000 times. (2) The inlet valve was closed after the subgrade soil was saturated, without providing continuous water source.

After the test, we divided the Lean Clay into 5 layers and performed particle gradation analysis on each layer. The results are shown in Fig. 8 (the gradation curves of the fourth and fifth layers of Lean Clay are highly coincident with those of the Lean Clay before the test, which are no longer shown in the Fig. 8). After the test, we see that fine particle content (particle size less than 0.075 mm) in the first layer is significantly increased, while fine particle content in the second layer is significantly reduced. This content in the third layer is slightly reduced, indicating that the fine particles migrate upward from the middle to the upper part of the subgrade soil.

3.2 The influence of cyclic loading amplitude

Fig. 9 shows the influence of cyclic loading amplitude on axial strain and excess pore water pressure during testing. Here we see that the axial strain of the samples under different cyclic loading amplitude presents a consistent trend: it first increases rapidly and then increases slowly. As the cyclic loading amplitude increases, the axial strain increases. When the cyclic loading amplitude is 50 kPa, 100 kPa, and 200 kPa, the final axial strains of the samples are 2.49%, 3.00%, and 5.03%, respectively. The curves of excess pore water pressure show a rapid increase to the maximum value and then a gradual decrease. With the increase in cyclic loading amplitude, the excess pore water pressure generated at point B gradually increases.

3.3 The influence of loading frequency

We plot the influence of loading frequency on the axial strain, the excess pore water pressure during the mud pumping

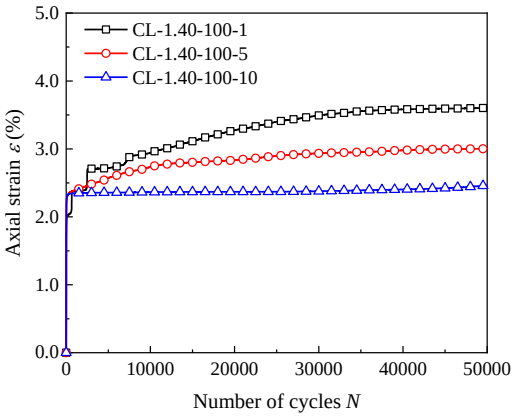

(a) Axial strain

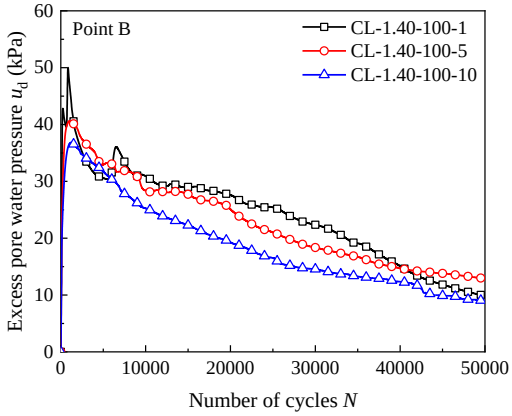

(b) Excess pore water pressure (point B)

Fig. 10 The influence of loading frequency

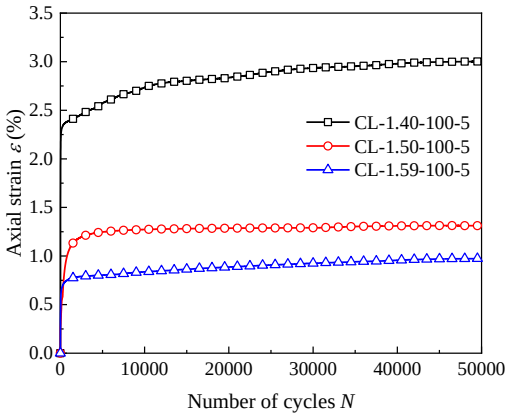

(a) Axial strain

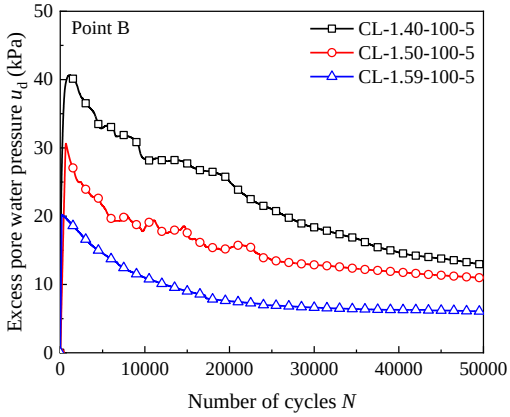

(b) Excess pore water pressure (point B)

Fig. 11 The influence of initial dry density

test in Fig. 10. From Fig. 10, we can see that the loading frequency has a significant effect on the axial strain: the axial strain of the sample gradually decreases with the increase in the loading frequency. The loading frequency has a relatively small effect on excess pore water pressure, but it still displays a certain pattern. That is, as the loading frequency increases, the excess pore water pressure for the same number of cycles decreases. From our experiment, we see that the increase in loading frequency does not aggravate the degree of mud pumping, but can significantly shorten the progress of mud pumping. In other words, with an increase in frequency, the time required for the same number of vibrations will also be shorter.

3.4 The influence of initial dry density

Fig. 11 shows the influence of the initial dry density of Lean Clay subgrade (ρ_d =1.40 g/cm^3, 1.50 g/cm^3, 1.59 g/cm^3) on the mud pumping test results. Here we see that as the initial dry density increases, the axial strain of the sample gradually decreases. At the end of the test, the axial strain of the sample with the initial dry density of 1.40 g/cm^3 was 3.0%, while the axial strain generated with the initial dry density of 1.50 g/cm^3 and 1.59 g/cm^3 was 1.3% and 0.9%, respectively. With the increase in the initial dry density, the excess pore water pressure for a given number of cycles gradually decreases.

3.5 Analysis of mud pumping degree

We selected four reference points (point 1 to point 4) for each group of tests, and recorded the height of mud during the test (number of cycles N=1,000, 15,000, and 30,000) and after the test (N=50,000), as well as the thickness of the interlayer, as shown in Table 3. Table 3 shows that the height of mud at each observation point increases gradually with the increase in loading times. Mud pumping mainly occurs in the early stage of cyclic loading (when the number of cycles is less than 15,000), and the degree of mud pumping gradually decreases in the late stage of cyclic loading. With an increase in cyclic loading amplitude, the height of mud and the thickness of the interlayer increase gradually, but with the increase in the initial dry density of Lean Clay subgrade, the height of mud and the thickness of the interlayer decrease gradually. The effect of loading frequency on the height of mud and the thickness of the interlayer is insignificant.

3.6 Fouling of gravel after the test

After the test, we divide the gravel into three layers (layer I, layer II, and layer III from top to bottom). The thickness of layer I and layer II is 50 mm, and the thickness of layer III is 30 mm. After drying, we weighed the gravel, and then cleaned it to remove the silt clay mud adhered to it. After drying again, we carried out particle sieving in order to obtain the gradation curves of each layer of gravel, and the gradation curves of gravel after the test are shown in Fig. 12. The total

Table 3 Mud pumping height and interlayer thickness

No.	The height of mud height at point 1/ mm				The height of mud height at point 2/ mm			
	N=1000	15000	30000	50000	*N*=1000	15000	30000	50000
CL-1.40-50-5	11.0	12.0	12.0	12.0	8.0	11.0	16.0	18.0
CL-1.40-100-1	18.0	21.0	22.0	22.0	24.0	26.0	27.0	27.0
CL-1.40-100-5	27.0	30.0	32.0	33.0	6.0	25.0	28.0	32.0
CL-1.40-100-10	13.0	17.0	17.0	17.0	15.0	20.0	22.0	22.0
CL-1.40-200-5	30.0	31.0	32.0	34.0	33.0	36.0	36.0	36.0
CL-1.50-100-5	22.0	24.0	25.0	26.0	11.0	12.0	13.0	13.0
CL-1.59-100-5	5.0	10.0	15.0	15.0	3.0	5.0	5.0	5.0

No.	The height of mud height at point 3/ mm				The height of mud height at point 4/ mm				Interlayer thickness/ mm
	N=1000	15000	30000	50000	*N*=1000	15000	30000	50000	
CL-1.40-50-5	2.0	3.0	3.0	3.0	8.0	11.0	12.0	12.0	7.0
CL-1.40-100-1	20.0	23.0	24.0	24.0	18.0	28.0	28.0	28.0	12.0
CL-1.40-100-5	11.0	12.0	12.0	13.0	15.0	17.0	20.0	21.0	10.0
CL-1.40-100-10	8.0	17.0	25.0	25.0	10.0	12.0	20.0	21.0	10.0
CL-1.40-200-5	22.0	25.0	26.0	26.0	16.0	16.0	16.0	16.0	14.0
CL-1.50-100-5	11.0	12.0	12.0	13.0	14.0	15.0	15.0	16.0	5.0
CL-1.59-100-5	5.0	7.0	8.0	8.0	2.0	3.0	3.0	3.0	2.0

Table 4 The mass of the mud after the test

No.	Mass of mud/ g
CL-1.40-50-5	235.0
CL-1.40-100-1	433.0
CL-1.40-100-5	422.8
CL-1.40-100-10	365.0
CL-1.40-200-5	499.6
CL-1.50-100-5	166.2
CL-1.59-100-5	115.1

mass of Lean Clay mud inside the gravel layer under different conditions is listed in Table 4. The particles with a size of 1.0-8.0 mm were primarily derived from gravel particle breakage, and the particles with a size less than 1.0 mm were primarily derived from the migration of fine particles in the subgrade soil and gravel particle abrasion. The proportion of particle abrasion was relatively minimal because the loss rate of gravel mass before and after the test was less than 1.0%. Thus, we only consider that the particles with a size less than 1.0 mm were caused by the migration of fine particles (slurry).

Figs. 12 and Table 4 show that the gradation curves of gravel of layer I after the test basically overlap with those from before the test, indicating that there is no mud in layer I. The gradation curves of gravel in layer II and layer III deviate to the upper right compared with the gradation curve of gravel before the test, indicating that there were fine particles (including the fine particles produced by particle breakage under cyclic load and the Lean Clay mud that comes up from the subgrade) in gravel layer II and III. In addition, the degree of deviation of the gradation curves of the gravel in layer III is greater, indicating that the mud in layer III is much more than that in layer II. In general, with the increase in cyclic loading amplitude, the mass of mud after the test gradually increases, and with the increase in loading frequency and initial dry density of subgrade, the mass of mud decreases. Hence, we find evidence that increasing the initial dry density of subgrade soil can mitigate the problem of subgrade mud pumping, but increasing train axle load can aggravate the problem of subgrade mud pumping.

3.7 Treatment measures of subgrade mud pumping

How to effectively solve the mud pumping problem has become an important research topic in recent years. At present, the main treatment measures of mud pumping are: (1) clearing the ballast or removing the mud pumping subgrade soil, replacing the ballast or high-quality subgrade filler; (2) strengthening subgrade drainage; (3) laying geosynthetics; (4) chemical reinforcement method. The cost of (1) is generally high, and some chemical reinforcement agents used in chemical reinforcement methods may cause certain damage to the environment. As an economic, environmental protection and effective treatment measure, strengthening subgrade drainage and geosynthetics are widely used in the treatment of railway subgrade mud pumping.

The authors use the above test model to analyze the influence of various water levels on the characteristics of subgrade mud pumping (Ding *et al.* 2022a), and find that when the water level is 50 mm lower than the subgrade soil surface, the degree of fine particle migration can be significantly inhibited, and the issues of subgrade mud pumping no longer exist. Similarly, the authors analyze the inhibition effect of geotextiles laid between subgrade and ballast layer on the migration of fine particles (Ding *et al.* 2022b), we find that the addition of geotextile can effectively mitigate subgrade

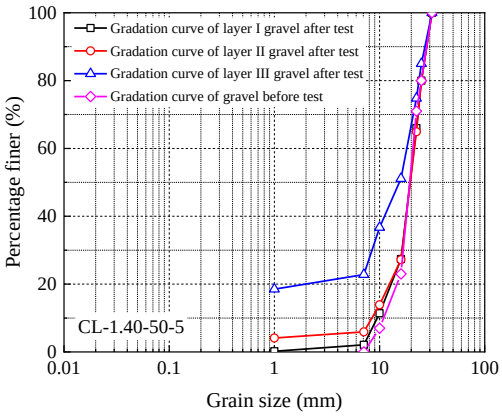

(a) CL-1.40-50-5

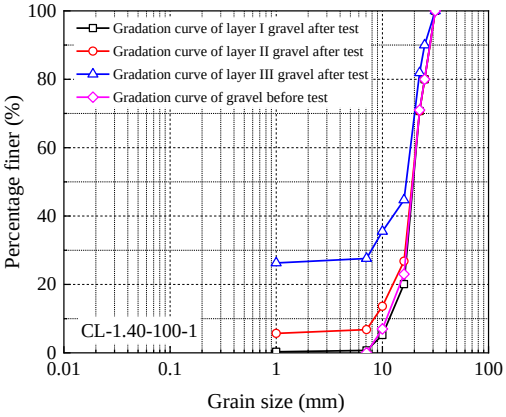

(b) CL-1.40-100-1

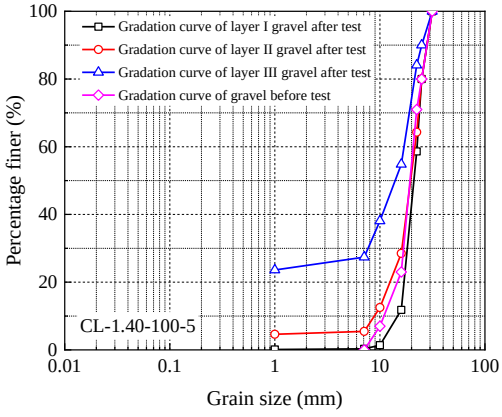

(c) CL-1.40-100-5

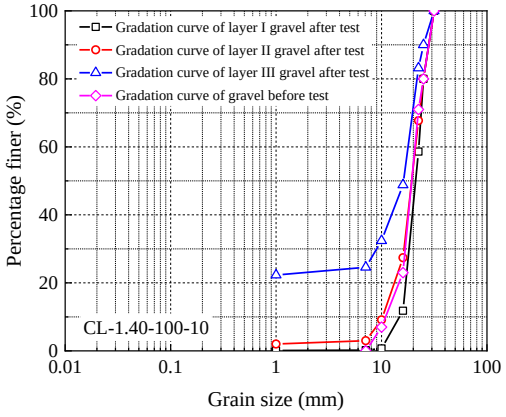

(d) CL-1.40-100-10

Fig. 12 Gradation curves of gravel after the test

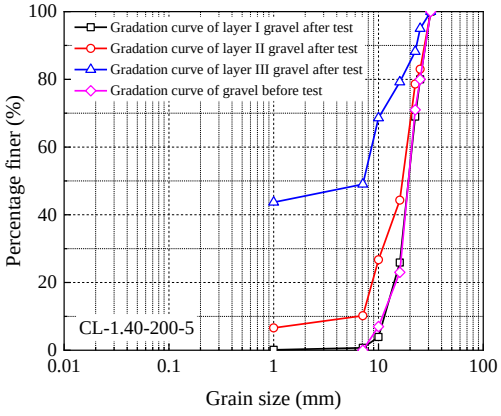

(e) CL-1.40-200-5

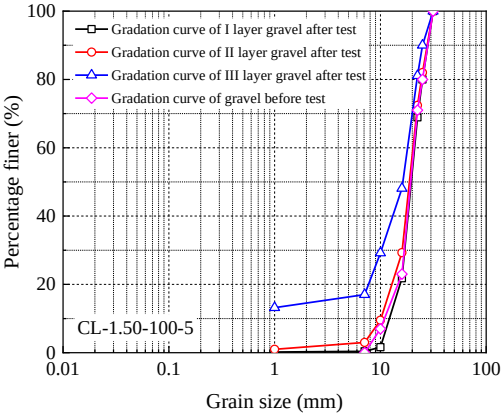

(f) CL-1.50-100-5

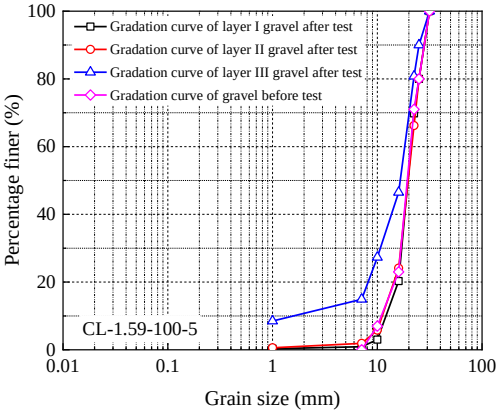

(g) CL-1.59-100-5

Fig. 12 Continued-

mud pumping. However, with an increase in cyclic loading amplitude, the mitigating effectiveness of geotextile on the mud pumping gradually weakens, and its long-term effectiveness needs to be further studied.

4. Discussion on the mechanism of mud pumping in Lean Clay subgrade

Here, we define the excess pore water pressure gradient ($i_{d,ij}$) as the ratio of the water head difference between the two points and the distance between the two points (Arivalagan *et al.* 2021), as shown in Eq. (3).

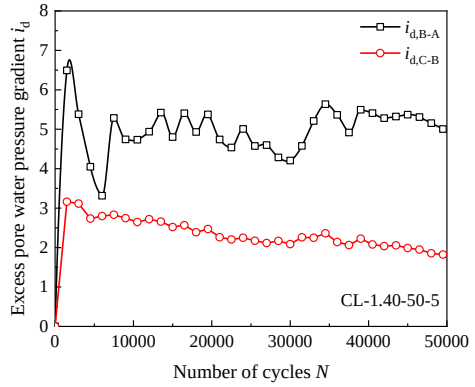

(a) CL-1.40-50-5

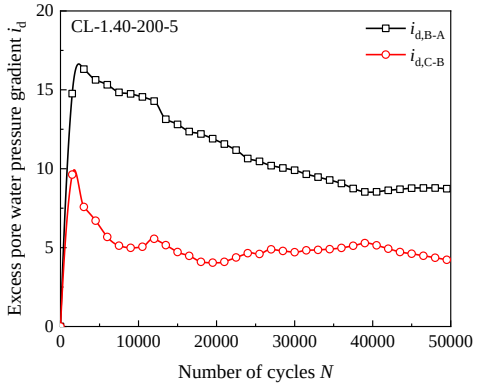

(b) CL-1.40-200-5

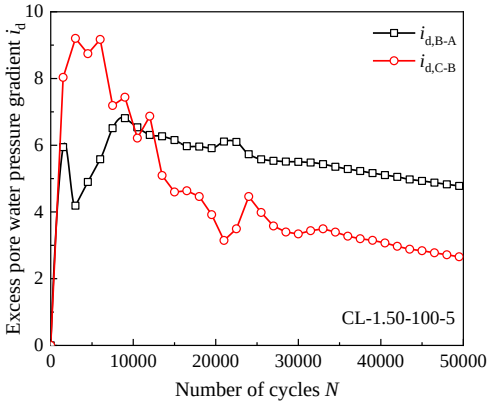

(c) CL-1.50-100-5

Fig. 13 Curves of the excess pore water pressure gradient

$$i_{d,ij} = \frac{u_{dj} - u_{di}}{\rho_w g L_{ij}} \tag{3}$$

where, u_{di} and u_{dj} are the excess pore water pressure between pionts i and j, ρ_w is the density of water, g is acceleration of gravity, and L_{ij} is the distance between points i and j.

Fig. 13 shows the curves of the excess pore water pressure gradient with the number of cycles in the CL-1.40-50-5, CL-1.40-200-5 and CL-1.50-100-5 tests. Here we see that the excess pore water pressure gradient increases first and then gradually decreases with the increase in the number of cycles. After 50,000 cycles, the excess pore water pressure gradient for B-A is still greater than 5.0, which is enough to cause the fine particles in the subgrade to migrate, and cause mud pumping. In addition, Fig. 13 also shows that the excess pore water pressure gradient for B-A is larger than that for C-B, indicating that the migration of fine particles mainly occurs in the middle and upper part of the subgrade soil, which is consistent with the conclusion obtained from Fig. 7. It should be noted that in Fig. 13(c), when the number of cycles is between 1500 and 10000 times, the excess pore water pressure gradient for C-B is greater than that for B-A, so there are errors inthe test data at this time. As mentioned above, the sensor at point A is located below the interface between the gravel layer and the subgrade. During cyclic loading, gravel particles that penetrate into the subgrade can impact the precision of the pore water pressure sensor's readings.

Based on the above analysis, we find that the upward excess pore water pressure gradient under cyclic loading drives the upward migration of fine particles (mud), which is the phenomenon of mud pumping. In addition, we also find that the mud pumping occurs simultaneously with the generation of an interlayer, and the interlayer has an exacerbatory effect on mud pumping (Duong *et al.* 2014b).

5. Conclusions

In this paper, we designed a new test model to study the characteristics of subgrade mud pumping. This model can monitor the evolution of subgrade mud pumping, excess pore water pressure, and dynamic stress in soil under cyclic loading. Using this test model, we obtained the following conclusions:

1) Under the action of cyclic loading, the curves of axial strain of the sample plotted against the number of cycles show a rapid increase and then slow increase. The curves of the excess pore water pressure with number of cycles show a rapid increase and then slow decrease. The dynamic stress in soil first increases rapidly and then decreases slowly.

2) The axial strain for a given number of cycles increases with an increase in cyclic loading amplitude and decreases with an increase in the loading frequency and the initial dry density of Lean Clay. The excess pore water pressure increases with an increase in the cyclic loading amplitude and decreases with an increase in the initial dry density and is less affected by the loading frequency.

3) An increase in the initial density of subgrade soil can mitigate the problem of subgrade mud pumping but that increasing train axle load can aggravate the problem of subgrade mud pumping. Although an increase in train speed cannot aggravate the degree of mud pumping, it can shorten the time of mud pumping.

4) The upward excess pore water pressure gradient under cyclic loading drives the upward migration of fine particles (mud), and cause mud pumping. In addition, the generation of an interlayer has an exacerbatory effect on mud pumping.

Acknowledgements

The study was supported by the the Science and Technology Research and Development Program of China

National Railway Group Corporation Limited. Project (L2022G002). The authors are grateful for the anonymous reviewers for their constructive comments and suggestions. The authors thank AiMi Academic Services (www.aimieditor.com) for the English language editing and review services.

References

Abeywickrama, A., Indraratna, B. and Rujikiatkamjorn, C. (2019), "Excess pore-water pressure generation and mud pumping in railways under cyclic loading", *Geotechnics for Transportation Infrastructure Infrastructure, Lecture Notes in Civil Engineering*, **28**, 371-383. https://doi.org/10.1007/978-981-13-6701-4_24.

Alobaidi, I. and Hoare, D.J. (1999), "Mechanisms of pumping at the subgrade-subbase interface of highway pavements", *Geosynthetics Int.*, **6**(4), 241-259. https://doi.org/10.1680/gein.6.0152.

Arivalagan, J., Rujikiatkamjorn, C., Indraratna, B. and Warwick, S. (2021), "The role of geosynthetics in reducing the fluidisation potential of soft subgrade under cyclic loading", *Geotext. Geomembranes*, **49**, 1324-1338. https://doi.org/10.1016/j.geotexmem.2021.05.004.

Bian, X.C., Jiang, J.Q., Jin, W.F., Sun, D.D., Li, W. and Li, X.M. (2016), "Cyclic and postcyclic triaxial testing of ballast and subballast", *J. Mater. Civil Eng.*, **28**(7), 04016032. https://doi.org/10.1061/(ASCE)MT.1943-5533.0001523.

Boomintahan, S. and Srinivasan, G.R. (1988), "Laboratory studies on mud-pumping into ballast under repetitive rail loading", *Indian Geotech. J.*, **18**(1): 31-47.

Cai, Y.Q., Yan, S.H., Cao, Z.G. and Li, F.Y. (2021), "Experiments to investigate mechanism of mud pumping of road base on silty clay soil under cyclic loading", *J. Jilin University (Engineering and Technology Edition)*, **51**(5), 1742-1748. https://doi.org/10.13229/j.cnki.jdxbgxb20200455.

Cao, G., Wang, X. and He, C.D. (2023), "Dynamic analysis of a laterally loaded rectangular pile in multilayered viscoelastic soil", *Soil Dyn. Earthq. Eng.*, **165**: 107695. https://doi.org/10.1016/j.soildyn.2022.107695.

Chawla, S. and Shahu, J.T. (2016), "Reinforcement and mud-pumping benefits of geosynthetics in railway tracks: Model tests", *Geotext. Geomembranes*, **44**(3), 366-380. https://doi.org/10.1016/j.geotexmem.2016.01.005.

Chen, Z.G. (2016), "Research on the reinforcing design to the subgrade disease of Dazhun railway", Chengdu: Southwest Jiaotong University.

Ding, Y., Jia, Y., Wang, X., Zhang, J.S., Luo, H., Zhang, Y. and Chen, X.B. (2022a), "The characteristics of subgrade mud pumping under various water level conditions", *Geomech. Eng.*, **30**(2), 201-210. https://doi.org/10.12989/gae.2022.30.2.201.

Ding, Y., Jia, Y., Wang, X., Zhang, J.S., Luo, H., Zhang, Y. and Chen, X.B. (2022b), "The influence of geotextile on the characteristics of railway subgrade mud pumping under cyclic loading", *Transport. Geotech.*, **37**, 100831. https://doi.org/10.1016/j.trgeo.2022.100831.

Duong, T.V., Cui, Y.J., Tang, A.M., Dupla, J.C., Canou, J., Calon, N., Robinet, A., Chabot, B. and De, L.E. (2014a), "Physical model for studying the migration of fine particles in the railway substructure", *Geotech. Test. J.*, **37**(5), 895-906. https://doi.org/10.1520/GTJ20130145.

Duong, T.V., Cui, Y.J., Tang, A.M., Dupla, J.C., Canou, J., Calon, N. and Robinet, A. (2014b), "Investigating the mud pumping and interlayer creation phenomena in railway sub-structure", *Eng. Geol.*, **171**, 45-58. https://doi.org/10.1016/j.enggeo.2013.12.016.

Gao, F., He, X.Z. and Zhang, S. (2021), "Pumping effect of rainfall-induced excess pore pressure on particle migration", *Transport. Geotech.*, **31**, 100669. https://doi.org/10.1016/j.trgeo.2021.100669.

Han, B.W. (2018), "A study on dynamic wetting characteristics of heavy load railway subgrade soil", Shijiazhuang: Shijiazhuang Tiedao University.

Hasnayn, M.M., Mccarter, W.J., Woodward, P.K. and Connolly, D.P. (2020), "Railway subgrade performance after repeated flooding-Large-scale laboratory testing", *Transport. Geotech.*, **23**, 100329. https://doi.org/10.1016/j.trgeo.2020.100329.

He, C.D., Brijes, M., Yuan, W., Wang, X. and Shi, Q.W. (2024), "Investigation of the dynamic behavior and fracturing mechanism of granite", *Fuel*, **360**, 130579. https://doi.org/10.1016/j.fuel.2023.130579.

Hu, J.Z. (2003), "Analysis on the diseases of the expansive soil subgrade in the double track section of Jiaoliu railway", *Subgrade Eng.*, **5**, 15-17.

Hussaini, S.K.K., Indraratna, B. and Vinod, J.S. (2016), "A laboratory investigation to assess the functioning of railway ballast with and without geogrids", *Transport. Geotech.*, **6**, 45-54. https://doi.org/10.1016/j.trgeo.2016.02.001.

Indraratna, B., Attya, A. and Rujikiatkamjorn, C. (2009), "Experimental investigation on effectiveness of a vertical drain under cyclic loads", *J. Geotech. Geoenviron. Eng.*, **135**, 835-839. https://doi.org/10.1061/(ASCE)GT.1943-5606.0000006.

Indraratna, B., Ngo, N.T. and Rujikiatkamjorn, C. (2011), "Behavior of geogrid-reinforced ballast under various levels of fouling", *Geotext. Geomembranes*, **29**(3), 313-322. https://doi.org/10.1016/j.geotexmem.2011.01.015.

Indraratna, B., Rujikiatkamjorn, C., Ewers, B. and Adams, M. (2010), "Class A prediction of the behavior of soft estuarine soil foundation stabilized by short vertical drains beneath a rail track", *J. Geotech. Geoenviron. Eng.*, **136**, 686-696. https://doi.org/10.1061/(ASCE)GT.1943-5606.0000270.

Indraratna, B., Tennakoon, N., Nimbalkar, S. and Rujikiatkamjorn, C. (2013), "Behaviour of clay-fouled ballast under drained triaxial testing", *Géotechnique*, **63**(5), 410-419. https://doi.org/10.1680/geot.11.P.086.

Indraratna, B., Wijewardena, L.S.S. and Balasubramaniam, A.S. (1993), "Large-scale triaxial testing of greywacke rockfill", *Géotechnique*, **43**(1), 37-51. http://doi.org/10.1680/geot.1994.44.3.539.

Kamruzzaman, A.H.M., Haque, A. and Bouazza, A. (2008), "Filtration behaviour of granular soils under cyclic load", *Géotechnique*, **58**(6), 517-522. https://doi.org/10.1680/geot.2007.00020.

Koohmishi, M. and Azarhoosh, A. (2020), "Assessment of drainage and filtration of sub-ballast course considering effect of aggregate gradation and subgrade condition", *Transport. Geotech.*, **24**, 100378. https://doi.org/10.1016/j.trgeo.2020.100378.

Liu, J.K. and Xiao, J.H. (2010), "Experimental study on the stability of railroad silt subgrade with increasing train speed", *J. Geotech. Geoenviron. Eng.*, **136**(6), 833-841. https://doi.org/10.1061/(asce)gt.1943-5606.0000282.

Liu, S. (2021), "Study on the mechanism of mud-pumping of high-speed railway subgrade and its caused wheel-rail dynamic responses," Jinan: Shandong University.

Miao, L.Q., Yue, Z.R. and Feng, H.P. (2014), "Causes and prevention measures of mud pumping in existing heavy haul railways subgrade", *Anhui Architect.*, **20**(1), 113-121.

Nguyen, T.T. and Indraratna, B. (2021), "Rail track degradation under mud pumping evaluated through site and laboratory investigations", *Int. J. Rail Transport.*, 1-28. https://doi.org/10.1080/23248378.2021.1878947.

Nguyen, T.T., Indraratna, B. and Phan, N.M. (2019), "Mud pumping under railtracks: mechanisms, assessments and solutions", *Aust. Geomech. J.*, **54**(4), 59-80.

PHAM, D.P. (2015), "Study on the mud pumping mechanism and reinforcement effect for graded gravel in high-speed railway ballastless track surface layer of subgrade bed", Chengdu: Southwest Jiaotong University.

Sun, Q.D., Indraratna, B. and Nimbalkar, S. (2016), "Deformation and degradation mechanisms of railway ballast under high frequency cyclic loading", *J. Geotech. Geoenviron. Eng.*, **142**(1), 04015056. https://doi.org/10.1061/(ASCE)GT.1943-5606.0001375.

Takatoshi, I. (1997), "Measures for stabilization of railway earth structures", Japan railway technical service.

TB10102-2010 (2010), "Code for soil test of railway engineering", Beijing: China Railway Publishing House.

Tennakoon, N. and Indraratna, B. (2014), "Behaviour of clay-fouled ballast under cyclic loading", *Geotechnique*, **64**(6), 502-506. https://doi.org/10.1680/geot.13.T.033.

Tennakoon, N., Indraratna, B., Rujikiatkamjorn, C., Nimbalkar, S. and Neville, T. (2012), "The role of ballast-fouling characteristics on the drainage capacity of rail substructure", *Geotech. Test. J.*, **35**(4), 629-640. https://doi.org/10.1520/gtj104107.

Touqan, M., Ahmed, A., Naggar, H.E. and Stark, T. (2020), "Static and cyclic characterization of fouled railroad sub-ballast layer behaviour", *Soil Dyn. Earthq. Eng.*, **137**, 106293. https://doi.org/10.1016/j.soildyn.2020.106293.

Trani, L.D.O. and Indraratna, B. (2010a), "Assessment of subballast filtration under cyclic loading", *J. Geotech. Geoenviron. Eng.*, **136**(11), 1519-1528. https://doi.org/10.1061/(ASCE)GT.1943-5606.0000384.

Trani, L.D.O. and Indraratna, B. (2010b), "Experimental investigations into subballast filtrations behaviour under cyclic conditions", *Aust. Geomech.*, **45**(3), 123-133.

Trinh, V.N., Tang, A.M., Cui, Y.J., Dupla, J.C., Canou, J., Calon, N., Lambert, L., Robinet, A. and Schoen, O. (2012), "Mechanical characterisation of the fouled ballast in ancient railway track substructure by large-scale triaxial tests", *Soils Found.*, **52**(3), 511-523. https://doi.org/10.1016/j.sandf.2012.05.009.

Wang, D.J. (2006), "Subgrade disease rectification of K497+650 ~ K497+850 section of Shuohuang railway", *Railway Constr. Technol.*, (1), 29-31.

Wang, H.L. (2017), "Mechanical characterization and moisture migration of the high-speed railway track-bed", Hangzhou: Zhejiang University.

Wheeler, L.N., Take, W.A. and Hoult, N.A. (2017), "Performance assessment of peat rail subgrade before and after mass stabilization", *Can. Geotech. J.*, **54**, 674-689. https://doi.org/10.1139/cgj-2016-0256.

Yang, Z.H. (2015), "Research on the mechanism of mud pumping of heavy haul-railways", Shijiazhuang: Shijiazhuang Tiedao University.

Yang, Z.H., Yue, Z.R. and Tai, B.W. (2021), "Investigation of the deformation and strength properties of fouled graded macadam materials in heavy-haul railway subgrade beds", *Constr. Build. Mater.*, **273**, 121778. https://doi.org/10.1016/j.conbuildmat.2020.121778.

Yin, C.F. (2012), "Inspection and analysis on subgrade defects over station throat at shenchi south of shuohuang railway", *Modernurban Transit*, (03): 65-67.

Zhang, S., Gao, F., Chen, Q.L. and Sheng, D.C. (2020), "Experimental study of fine particles migration mechanism of sand-silt mixtures under train load", *Rock Soil Mech.*, **41**(5), 1591-1598. https://doi.org/10.16285/j.rsm.2019.0690.

Zhou, H., He, C.D., Wang, X., Chen, Y.J. and Li, J. (2023), "Assessment of the seismic response of shallow buried elliptical tunnels", *J. Earthq. Eng.*, **27**(3), 465-487. https://doi.org/10.1080/13632469.2021.2009057.

GC